was the same for both methods. For the RKA method, zero initial condition was used and integration was carried out over many cycles until the convergence criterion of Eq. (2) was satisfied. Figure 1 clearly shows that the time for the SSA to produce a steady-state response is independent of both speed and damping, since all four cases lie on the same curve, unlike the RKA's obvious dependence upon these parameters. For the SSA, these errors fall well below the tolerance requirement for convergence [Eq. (2)]. Hence, Fig. 1 does not reflect the time required for both methods to produce the same error. In light of this figure, the SSA is clearly the better of the two methods.

In order to compare the different methods (SSA and EXPA), it was necessary to calculate the relative errors. The maximum relative errors were calculated by solving for y(0), integrating using the fourth-order Runge-Kutta method for 2 cycles, and finding the maximum relative error between the two cycles, $e_{r}^{!}$ [see Eq. (2)].

Figure 2 provides a comparison of SSA and EXPA with regard to the computation time for a desired accuracy. Several cases of EXPA were used for this comparison. EXPA2, EXPA3, EXPA4, and EXPA5 refer to the EXPA method using, respectively, j = 2, 3, 4, and 5 [Eq. (12)], in the Taylor series approximation to estimate the exponential of $[A_i]\Delta t$. In generating time/error plots, the number of intervals required to obtain a certain accuracy (based on e_r^1) were computed for each method. Then for the respective number of intervals, simulations were performed using a Gateway 2000 486 4DX-33 MHz personal computer, with 8 MB RAM. Figure 2 illustrates that the SSA method is more efficient in computation time. The enhancement in computation time offered by the SSA over the EXPA is increasingly more as the accuracy requirement is made more stringent (e_r^1 is required to be smaller). The improvement in computational time is essentially due to the accuracy of the SSA method in that for a desired e_r^1 , the SSA method requires a significantly smaller number of intervals than the EXPA method.

Conclusion

A new efficient method for calculating the steady-state response of linear systems with periodic coefficients has been presented. The method consists of two steps: (i) solve for the initial conditions that give steady-state behavior, and (ii) supply these initial conditions to a Runge-Kutta type integration scheme and integrate over a single cycle. Using a practical machinery example, the method has been compared to two other procedures in order to assess its computational efficiency. The method has been found to be significantly faster and more accurate than present methods.

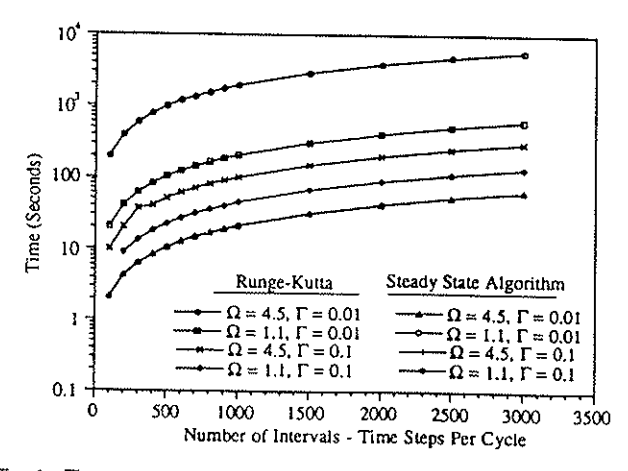


Fig. 1 Time comparison of SSA and RKA with various cases of speed and damping

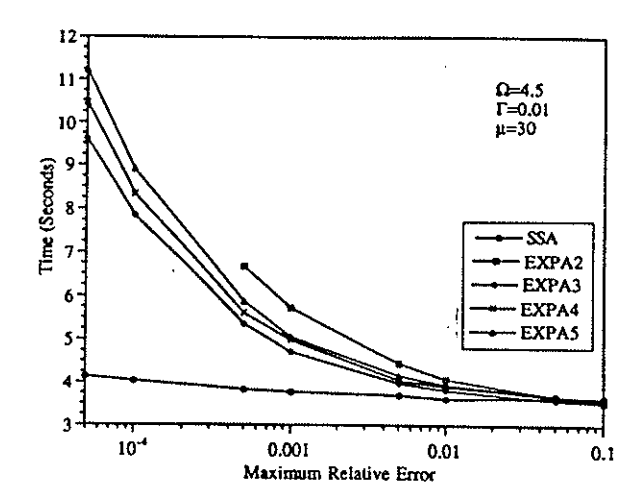


Fig. 2 Calculation time for prescribed errors of SSA and EXPA

Acknowledgments

This work was supported, in part, by the Materials Technology Center at Southern Illinois University.

References

Butcher, J. C., 1987, The Numerical Analysis of Ordinary Differential Equations, Wiley, New York, New York.

Cameron, T. M., and Griffin, J. H., 1989, "An Alternating Frequency/Time Domain Method for Calculating the Steady-State Response of Nonlinear Dynamic Systems," ASME Journal of Applied Mechanics, Vol. 56, pp. 149-154.

Chivate, P. N., and Farhang, K., 1993, "Effect of Coupler Material Damping on Steady-State Response Calculation of Elastic Mechanisms," Dynamics and Vibration of Time-Varying Systems and Structures, DE-Vol. 56, ASME, pp. 139-

Erdman, A. G., ed., 1993, Modern Kinematics: Developments in the Last Forty Years. Wiley, New York, New York.

Farhang, K., 1989, "Analytical and Experimental Parametric Vibration Stability Studies in Elastic Mechanisms," Ph.D. Dissertation, Purdue University, West Lafayette, Indiana.

Farhang, K., and Midha, A., 1995, "Steady-State Response of Periodically Time-Varying Linear Systems, With Application to an Elastic Mechanism, ASME Journal of Mechanical Design, Vol. 117, pp. 633-639.

Friedmann, P., Hammond, C. E., and Woo, T. H., 1977, "Efficient Numerical Treatment of Periodic Systems with Application to Stability Problems,* tional Journal of Numerical Methods in Engineering, Vol. 11, pp. 1117-1136.

Hsu, C. S., 1974, "On Approximating a General Linear Periodic System," Journal of Mathematics Analysis and Applications, Vol. 45, pp. 234-251. Rodrigues, P. J. C., Howes, M. J., and Richardson, J. R., "Efficient Computa-

tion of the Steady-State Response of Periodic Nonlinear Microwave Circuits Using a Convolution-Based Sample-Balance Technique," IEEE Transactions on Microwave Theory and Techniques, Vol. 39, pp. 732-737.
Sinha, S. C., and Wu, D. H., "An Efficient Computational Scheme for the

Analysis of Periodic Systems," Journal of Sound and Vibration, Vol. 151, pp.

Dispersion of Flexural Waves on Shells

D. A. Rebinsky¹ and A. N. Norris²

Simple and accurate approximations are given for the dispersion properties of flexural waves on curved shells in vacuo. The

¹² Department of Mechanical and Aerospace Engineering, Rutgers University, Piscataway, NJ 08855-0909

Contributed by the Technical Committee on Vibration and Sound for publicauon in the JOURNAL OF VIBRATION AND ACOUSTICS. Manuscript received May 1994. Associate Technical Editor: C. Fuller.

results apply to shells of arbitrary double curvature, and are valid over the full frequency range of interest, from very high down to values below the generalized ring frequency.

1 Introduction

Vibration and transport of energy on elastic shells can be decomposed into a super-position of distinct wave types, typically membrane and flexural as on a flat plate (we will not consider evanescent wave types here). The dispersive behavior of propagating waves for arbitrary shell geometry is then required. Several authors have investigated the dispersion relations for cylindrical shells at frequencies greater than ring, (Soedel, 1981; Pierce and Kil, 1990; Guo, 1994). Means et al. (1991) also provided asymptotic approximations which represent various regions of the wave-normal curve, i.e., the wavenumber plane at fixed frequency, for a cylindrical shell below the ring frequency. Some results have been reported for arbitrarily shaped shells, starting with Germogenova (1973) who derived a short wavelength dispersion relation for flexural waves. Pierce (1993) presented a single dispersion relation that includes all wave types, membrane and flexural, while Norris and Rebinsky (1994) derived separate relations for each wave type, the flexural agreeing with Germogenova's.

Here we derive an approximate but explicit expression for the wave-normal curve of flexural waves on an arbitrarily shaped shell over a wide frequency range.

2 Dispersion Relations

Consider a thin elastic shell of arbitrary shape with its dynamic behavior governed by a set of equations of motion derived by Pierce (1993) which is a generalization of the Donnell-Yu model for cylindrical shells. Any shell theory would be adequate but this model is the simplest. We consider straight-crested waves of constant frequency traveling in the direction n, with phase $e^{i(\xi_3-\omega_1)}$, s being the coordinate along n, or the arc-length on a ray path. Pierce's (1993) dispersion relation for a shell of arbitrary shape, as simplified by Norris and Rebinsky (1994), is

$$\left(\xi^{2} - \frac{2k^{2}}{1 - \nu}\right) \left[(\xi^{2} - k^{2})(\xi^{4} - \kappa^{4}) - \kappa^{4} \xi_{\text{ring}}^{2} + (1 - \nu^{2}) \frac{\xi^{2}}{r^{2} R_{\perp}^{2}} \right] - 2(1 + \nu) \frac{\xi^{2} k^{2}}{r^{2} R_{T}^{2}} = 0, \quad (1)$$

where k and κ are the longitudinal and flexural wavenumbers for a flat plate, respectively,

$$k^2 = m\omega^2/C, \quad \kappa^4 = m\omega^2/B. \tag{2}$$

Here, m is the areal density, $C = Eh/(1 - \nu^2)$ is the extensional stiffness, and $B = Cr^2$ is the flexural stiffness, where E is Young's modulus, ν is Poisson's ratio, h is the thickness, and r is the radius of gyration, $r^2 = h^2/12$. The ring frequency for the general shell is defined by $k = \xi_{\text{ring}}$, where (Pierce, 1993)

$$\xi_{\text{nng}}^2 = \frac{1}{R_I^2} + \frac{1}{R_H^2} + \frac{2\nu}{R_I R_H}, \tag{3}$$

and R_{I} and R_{II} are the principal radii of curvature. The remaining two radii of curvature in Eq. (1) and a third for later usage are defined as

$$\frac{1}{R_{*}} = \frac{n_{I}^{2}}{R_{I}} + \frac{n_{II}^{2}}{R_{II}}, \quad \frac{1}{R_{\perp}} = \frac{n_{I}^{2}}{R_{II}} + \frac{n_{II}^{2}}{R_{I}},
\frac{1}{R_{T}} = n_{I}n_{II} \left(\frac{1}{R_{II}} - \frac{1}{R_{I}}\right),$$
(4)

where n_l and n_{ll} are components of **n** along the directions of principal curvature. The dispersion relation can be rewritten in nondimensional form as

$$\left(y - \frac{2b\delta^2}{1 - \nu}\right) \left[(y - b\delta^2)(y^2 - 1) - \frac{1}{b} + \frac{(1 - \nu^2)y}{k^2 R_\perp^2} \right] - 2 \frac{(1 + \nu)y}{\kappa^2 R_T^2} = 0, \quad (5)$$

where \sqrt{y} is the surface wavenumber normalized with respect to the flexural wavenumber, b is a dimensionless frequency and δ is a shell parameter,

$$y = \xi^2/\kappa^2$$
, $b = \kappa^2/\xi_{\text{ring}}^2$, $\delta = r\xi_{\text{ring}}$. (6)

2.1 Membrane Waves. We have previously studied in some detail the dispersion equations characterizing membrane waves on elastic shells of arbitrary shape for large frequencies (Norris and Rebinsky, 1994). Membrane dispersion was also investigated and discussed by Pierce and Kil (1990) and Guo (1994). We now summarize our results (Norris and Rebinsky, 1994) concerning membrane waves for completeness.

It is clear from its definition in Eq. (6) that $\delta \ll 1$ for thin elastic shells. We can therefore analyze the roots by taking advantage of the smallness of δ in the dispersion relation (5). We note that $b\delta = 1$ at the ring frequency and therefore $b\delta^2 \ll 1$ for frequencies near ring. We first consider the root $y \approx b\delta^2$ corresponding to the quasi-longitudinal wavenumber for which Eq. (5) can be manipulated to

$$\xi_{ql}^2 \approx k^2 - \left(\frac{1}{R_{\parallel}} + \frac{\nu}{R_{\perp}}\right)^2,\tag{7}$$

where $R_{\rm E}$ (R_{\perp}) of Eq. (4) is the radius of curvature parallel (perpendicular) to the ray path. We next turn to the root $y \approx 2b\delta^2/(1-\nu)$, which yields the wavenumber for quasi-transverse shell waves. Equation (5) can then be approximated as

$$\xi_{qr}^2 \approx \frac{2k^2}{1-\nu} - \frac{4}{R_r^2}$$
 (8)

For a circular cylindrical shell, the approximations obtained by Guo (1994) yield those determined from Eqs. (7) and (8) by ignoring fluid loading, neglecting flexure $k^2r^2 \ll 1$, and setting $\xi_z/k \approx n_z$ where n_z is the component of n along the axis.

2.2 Flexural Waves. We have also previously studied flexural wave dispersion at high frequencies (Norris and Rebinsky, 1994) on doubly-curved shells. For cylindrical shells, Guo (1994) has developed a mid-to-high frequency approximation of flexural dispersion. Our main concern in this Technical Brief is in obtaining approximations for the flexural wavenumbers on doubly-curved shells which are uniformly valid for the full frequency range from ring to high frequencies. As we will see, the final result is also quite accurate at frequencies below ring. Flexural waves correspond to roots of Eq. (5) such that y = O(1), which is equivalent to $\xi \approx \kappa$, or

$$y^{4} - \left[1 - \frac{(1 - \nu^{2})}{k^{2}R_{\perp}^{2}}\right]y^{2}$$

$$-\left[\xi_{nng}^{2} + 2(1 + \nu)\left(\frac{1}{R_{\perp}^{2}} + \frac{1}{R_{T}^{2}}\right)\right]\frac{y}{\kappa^{2}} \approx 0. \quad (9)$$

where

$$\alpha = \kappa^2 \left[\left(\frac{1}{R_H} - \frac{1}{R_I} \right)^2 + \frac{2(1+\nu)}{R_{\perp}} \left(\frac{1}{R_I} + \frac{1}{R_H} \right) \right]^{-1}, \quad (11a)$$

$$\beta = 1 - \frac{(1 - \nu^2)}{k^2 R_\perp^2},\tag{11b}$$

and note that α represents a dimensionless frequency parameter, $\alpha \propto \omega$. The dimensionless parameter β also depends upon frequency, but it is more strongly influenced by the direction of propagation in comparison to α .

In solving Eq. (10), we need to consider separately the three cases $\beta > 0$, $\beta = 0$, and $\beta < 0$. Thus, when $\beta > 0$, the three roots of Eq. (10) are

$$\{y_1, y_2, y_3\}$$

$$= \left\{ \frac{2}{\sqrt{3}}\cos\phi, -\sin\phi - \frac{1}{\sqrt{3}}\cos\phi, \sin\phi - \frac{1}{\sqrt{3}}\cos\phi \right\}, \quad (12)$$

where

$$\phi = \frac{1}{3}\cos^{-1}\frac{3}{2\alpha\beta}\sqrt{\frac{3}{\beta}}, \quad 0 \le \Re\phi \le \frac{\pi}{6}.$$
 (13)

In general, $y_1 > 0 > y_3 > y_2$, while the limiting values of the roots for large values of α are $y_1 \to 1$, $y_2 \to -1$, $y_3 \to 0$, as α \rightarrow ∞ . Hence, the propagating and evanescent quasi-flexural waves are given by the roots y_1 and y_2 , respectively. Both are well described by the flat plate limits of $y_1 = 1$, and $y_2 = -1$, except at very low frequencies where α is of order unity. Their approximate dispersion relations. Eqs. (12) and (13), perform well over the whole frequency range of interest, from $\alpha = O(1)$ to infinity. The root y₃ corresponds to the quasi-longitudinal wave which is evanescent at low frequencies. The fourth root of Eq. (9), $y_4 = 0$, represents the quasi-shear wave at low frequencies. For higher frequencies (i.e., above ring), the approximations (7) and (8) are more suitable for the quasi-longitudinal and quasi-shear wavenumbers than those based upon Eq. (9) or (10).

As previously stated, we are primarily concerned with the propagating quasi-flexural root y_1 , for which Eqs. (12) and (13) imply that

$$\left(\frac{\xi_{ef}}{\kappa}\right)^2 \approx 2\sqrt{\frac{\beta}{3}}\cos\left(\frac{1}{3}\cos^{-1}\frac{3}{2\alpha\beta}\sqrt{\frac{3}{\beta}}\right), \quad \beta > 0. \quad (14)$$

When β equals zero the quasi-flexural root is

$$\xi_{qf} \approx \kappa \alpha^{1/6}, \quad \beta = 0.$$
 (15)

As β becomes increasingly negative the assumption that y =O(1) for Eq. (9) is less accurate, with y becoming small and approaching $O(b\delta^2)$. Even so, we can obtain an approximation valid for the case when β is negative but only slightly so,

$$\left(\frac{\xi_{qt}}{\kappa}\right)^2 \approx 2\sqrt{\frac{|\beta|}{3}} \sinh\left(\frac{1}{3}\sinh^{-1}\frac{3}{2\alpha|\beta|}\sqrt{\frac{3}{|\beta|}}\right).$$

 $\beta < 0$. (16)

Expressions Eqs. (14) through (16) provide uniform approximations at the ring frequency as compared to that obtained previously for high frequencies (Norris and Rebinsky, 1994).

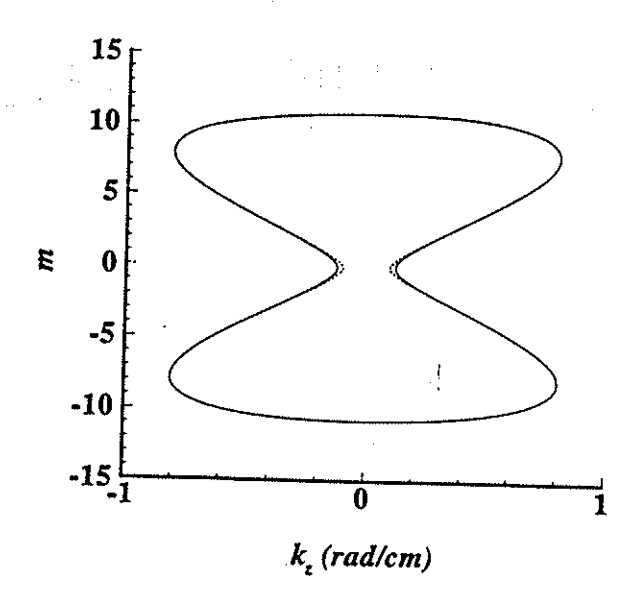


Fig. 1 Helical wavenumber diagram for 4871 Hz, where the ring frequency is 15168 Hz. The solid curve is the approximation (14) through (16) and the dashed line is the exact dispersion relation (1). Here, $k_{\rm c}$ ξ_{q} , cos θ and $m=\xi_{q}$, a sin θ where a is the cylinder radius and θ is angle between propagation direction and the axial direction.

Numerical Results

We consider a circularly cylindrical steel shell in vacuo, with $1/R_I = 0$, $R_{II} = 0.055$ m, and thickness $h = 5.3 \times 10^{-4}$ m, implying a ring frequency of 15168 Hz. This example corresponds to the cylindrical shell used by Williams et al. (1990) and Means et al. (1991). Rays traveling on an infinite cylindrical shell form helical paths. As the direction of propagation $(n_l,$ n_{II}) is varied for frequencies below ring, the helical wavenumber diagram for the flexural traveling wave forms the shape of a 'figure eight'' (Williams et al., 1990; Fahy. 1985).

Following Williams et al. (1990) and Means et al. (1991), we consider the frequency 4871 Hz, which is approximately one third of the ring frequency. A comparison of the quasiflexural wavenumber diagram calculated using the approximations (14) through (16) versus the "exact" dispersion relation given by Eq. (1) is shown in Fig. 1. Both expressions display the characteristic "figure eight" pattern. The parameter β becomes increasingly negative as the propagation direction approaches the cylinder axis $(m \approx 0)$, so it is not unexpected that the approximation (16) overestimates the helical wavenumber in this region. Note that Eq. (16) is derived on the assumption that $|\beta|$ is small. Generally, the difference between the asymptotic and exact wavenumbers is negligible for most directions of propagation of the helical wave.

Acknowledgment

This study was supported by the Office of Naval Research.

References

Fahy, F., 1985, Sound and Structural Vibration. Academic Press, New York. Germogenova, O. A., 1973, "Geometrical Theory of Flexure Waves in Shells." Journal of the Acoustical Society of America. Vol. 53, pp. 535-540. Guo. Y. P., 1994, "Approximate Solutions of the Dispersion Equation for

Fluid-Loaded Cylindrical Shells," Journal of the Acoustical Society of America. Vol. 95, pp. 1435-1440.

Means, S. L., Kouzoupis, S., and Pierce, A. D., 1991, "Wave Theory of Fluid-Loaded Cylindrical Shells Below the Ring Frequency," Structural Acoustics, NCA-Vol. 12/AMD-Vol. 128, pp. 235-242.

Norris, A. N., and Rebinsky, D. A., 1994, "Membrane and Flexural Waves on Thin Shells." ASME JOURNAL OF VIBRATION AND ACOUSTICS, Vol. 116, pp. 457Pierce, A. D., 1993, "Waves on Fluid-Loaded Inhomogeneous Elastic Shells of Arbitrary Shape," ASME JOURNAL OF VIBRATION AND ACOUSTICS, Vol. 115, pp. 384–390.

Pierce, A. D., and Kil. H.-G., 1990, "Elastic Wave Propagation from Point Excitations on Thin-Walled Cylindrical Shells," ASME JOURNAL OF VIBRATION AND ACOUSTICS, Vol. 112, pp. 399-406.

Soedel, W., 1981, Vibrations of Plates and Shells, Marcel Dekker, New York, Williams, E. G., Houston, B. H., and Bucaro, J. A., 1990, "Experimental Investigation of the Wave Propagation on a Point-Driven, Submerged Capped Cylinder using K-space Analysis," Journal of the Acoustical Society of America, Vol. 87, pp. 513-522.

Sensitivity Calculations for Broad-Band Acoustic Radiated Noise Design Optimization Problems

S. A. Hambric¹

Introduction

A new optimization methodology for solving broad-band radiated noise design problems has been developed (Hambric, 1995). The optimizer, called STRACOPT (STRuctural ACoustic OPTimizer), repeatedly manipulates design parameters, such as plating thicknesses and material loss factors, and executes numerical analysis programs until a design which meets radiated noise goal levels and has the lowest possible design objectives is found. The integration of optimization techniques and numerical structural/acoustic response prediction tools, such as the finite element method (FEM), allows a noise control engineer to investigate a large range of design alternatives in an efficient, productive manner. STRACOPT is applicable to a broad class of problems, including quieting machinery in industrial environments, reducing far-field radiated noise signatures of submerged military vehicles, and reducing interior noise levels in automobiles and aircraft.

The optimization process depends strongly on the accuracy and applicability of the design sensitivities, which indicate the effects of changing design parameters on design objectives and constraints. For broad-band radiated noise design optimization, the sensitivities of one-third octave radiated noise levels with respect to structural (plate thicknesses) and material (mass densities, loss factors) parameters are required. Since most FEM structural-acoustic analysis programs do not automatically compute radiated noise design sensitivities, finite difference approximations must be used to compute the sensitivities. Small perturbations of the design parameters are made, and the perturbed FEM models are reanalyzed. The sensitivities are then approximated using the differences in the radiated noise response and the size of the design variable perturbations. Since the accuracy of the finite difference approximation is directly related to the design parameter step size, the choice of step size may influence the likelihood of the optimization converging to a feasible design. Broad-band radiated noise design sensitivities may also be dependent on the frequency resolution used in the analyses. A coarse narrow-band response spectrum may be inadequate to resolve peaks in frequency response, which will lead to erroneous one-third octave band levels. Errors in the broad-band response will lead to errors in the sensitivities, which may hinder or prevent the optimizer from finding a feasible or optimal design.

This study therefore investigates the sensitivity analysis of broad-band radiated noise for various structural design parameters and the influence of the sensitivities on the optimization convergence characteristics of the STRACOPT capability. A better understanding of the influence of design sensitivity parameters (design parameter step size, frequency response resolution) on broad-band radiated noise sensitivities will lead to improved optimization success rates for broad-band radiated noise design optimization problems. The effectiveness of the sensitivities and optimization methods is measured by robustness (finding the global or near global minimum independent of starting design point) and computational efficiency (based on the required number of actual design evaluations). A finite element model of a submerged, ribbed cylindrical shell with hemispherical ends is used as a test case for the sensitivity and approximation methods. Design variable deltas and frequency response resolutions are varied to investigate their influence on the sensitivities and optimization robustness and efficiency.

Summary of Optimization Approach

The basic optimization approach using approximation functions (either first-order Taylor or half-quadratic series [second-order Taylor without cross terms]), design history weighting, and simulated annealing search is described in the earlier paper (Hambric, 1995). The approach is summarized below.

- 1. Create a composite objective function composed of multiple design criteria, such as structural weight and damping treatment cost. The objective function components may be individually weighted.
- 2. Augment the composite objective function with one-third octave band radiated noise constraints. When radiated noise levels exceed those of specified goal levels, a penalty function based on the amount of the goal violation in dB is used to add to the objective function.
- 3. Approximate radiated noise constraints using low-order series functions. First-order Taylor or half-quadratic approximations may be used to simulate the one-third octave band radiated noise levels over the design space.
- 4. Improve the approximations of the radiated noise design space by retaining the actual numerically-computed radiated noise levels from prior design iterations.
- 5. Globally search the approximate design space using simulated annealing to find the design with the lowest objective. If no feasible design is found, the global search will produce the least penalized design possible, effectively minimizing the radiated noise goal violations.
- 6. Repeat the procedure until design variable changes converge within a user-specified tolerance or repeat a design found in a previous iteration.

Design Sensitivities

The first- and second-order gradients used in the approximation functions for radiated noise are computed using finite difference equations, where the design variable vector is perturbed slightly and the FEM radiated noise analysis is repeated. The gradient computation, or sensitivity analysis, is typically the most computationally intensive component of design optimization. Each complete sensitivity analysis requires a number of FEM radiated noise evaluations equal to the number of design variables for the first-order approximations and twice the number of design variables for the half-quadratic approximations. (A full second-order Taylor series expansion would require a

Computational Mechanics Office (Code 204), NSWC, Carderock Division, Bethesda, MD

Contributed by the Technical Committee on Vibration and Sound for publication in the JOURNAL OF VIBRATION AND ACOUSTICS. Manuscript received Feb. 1995. Associate Technical Editor: G. H. Koopmann.